

**ARTIFICIAL INTELLIGENCE OF THINGS (AIOT) ENABLED  
E-VEST FOR REMOTE AND CONVENIENT ADOLESCENT  
IDIOPATHIC SCOLIOSIS DIAGNOSIS**

by

**FAN GAOYIGE**  
*(A0232682E)*

**A REPORT SUBMITTED FOR**

**EE5003 PROJECT**

in

**DEPARTMENT OF ELECTRICAL & COMPUTER ENGINEERING**

in the

**NATIONAL UNIVERSITY OF SINGAPORE**

**2022**

Supervisor:  
Assoc. Prof. Vincent Lee CK

Examiners:  
Dr. John Ho SY

## Acknowledgments

First of all, I would like to thank Prof. Lee Chengkuo, as my EE5003 supervisor, for taking time between his busy academic work to guide me in my project and providing many suggestions, which greatly improved my academic ability. Prof. Lee is a rigorous and knowledgeable scholar, sincere and open-minded, and his high level academic vision and dedicated work ethic have set an example for me. In addition, I would also like to thank Prof. Lee's PhD student, Mr. Sun Zhongda, who personally guided me through the experimental design during my year at NUS, helping me to develop my own academic thinking skills gradually after being overwhelmed at the beginning.

Moreover, I would like to send my thank to my partner, Zhou Jinfeng, who has helped me with the fabrication of sensor and the collection of data during my research with great patience. Without his help, I cannot realize many design in my project.

In the end, I would like to extend my thank to my parents and my family for the material and spiritual encouragement which enabled me to successfully complete my studies.

# Contents

<b>Acknowledgments</b>	<b>i</b>
<b>Abstract</b>	<b>iv</b>
<b>List of Figures</b>	<b>v</b>
<b>List of Tables</b>	<b>vii</b>
<b>1 Introduction</b>	<b>1</b>
1.1 Overview . . . . .	1
1.2 Innovation and Motivation . . . . .	3
1.3 Report Synopsis . . . . .	3
<b>2 Front-End Design</b>	<b>4</b>
2.1 E-Vest Design . . . . .	4
2.1.1 Vest Fabrication . . . . .	4
2.2 Sensor Fabrication . . . . .	5
2.2.1 Triboelectric Sensor . . . . .	5
2.2.2 Interdigitated Sensor . . . . .	13
2.2.3 Distribution on Vest . . . . .	15
2.3 Signal Acquisition Module . . . . .	16
2.3.1 BLE Communication . . . . .	17
2.3.2 Analog-Digital Convert . . . . .	17
2.4 Establishment of Data Set . . . . .	19
<b>3 Back-End Design</b>	<b>21</b>
3.1 App on phone . . . . .	21
3.1.1 BLE Connection . . . . .	22

3.1.2	Visualization . . . . .	24
3.2	Machine Learning . . . . .	25
3.2.1	Supported Vector Machine . . . . .	26
3.2.2	Random Forest . . . . .	27
3.2.3	Gradient Boosting Decision Tree . . . . .	28
3.2.4	XGBoost . . . . .	29
3.2.5	AdaBoost . . . . .	30
3.2.6	LightGBM . . . . .	31
3.2.7	Analysis and Conclusion . . . . .	32
3.2.8	Machine Learning on iPhone . . . . .	36
3.3	Database . . . . .	36
3.4	Web page . . . . .	37
3.4.1	Authorization . . . . .	38
3.4.2	Visualization . . . . .	38
3.4.3	Medical Instruction . . . . .	39
<b>4</b>	<b>Integration of System</b>	<b>40</b>
<b>5</b>	<b>Conclusion and Future Work</b>	<b>42</b>
5.1	Conclusion . . . . .	42
5.2	Further Research Directions . . . . .	42
<b>Bibliography</b>		<b>44</b>

## **Abstract**

Adolescent Idiopathic Scoliosis (AIS) is a skeletal-muscular disorder occurs in prepubescent or pre-mature skeletal growth. which causes great physical and psychological harm to the affected adolescents. Interventions to prevent the progression of AIS include exercise therapy, brace therapy and surgery. In this report, a solution based on brace therapy enabled by artificial intelligence of things for remote and convenient diagnosis is proposed. The solution consists of a 3d printed polyethylene undershirt customized for the patient's torso, sensors with integrated triboelectric and piezoresistive mechanisms and a signal acquisition module with low power Bluetooth transmission based on the NRF52810 chip. In order to facilitate data acquisition and analysis, the solution is based on the iOS platform and a mobile phone software is designed to collect the data sent by the undershirt in real time and upload it to the database. The software visualizes the collected data on the mobile phone. In addition, the software uses machine learning to recognize the user's posture in real time, with an accuracy of 100.0% for the classification of the six postures. Additionally, a cross-platform data analysis system was developed to assist patients with rehabilitation training and physician feedback guidance.

# List of Figures

2.1	The summarization of four basic working modes of TENG. . . . .	7
2.2	Fundamental principle of TENG. . . . .	8
2.3	Triboelectric series for some commonly materials following a tendency of easy losing electrons (positive) to gaining electrons (negative). . . . .	10
2.4	Working process of TENG under CS operation mode. . . . .	11
2.5	3D structure of the triboelectric sensor. . . . .	11
2.6	A picture of the real triboelectric sensor . . . . .	12
2.7	3D-printed molds for EcoFlex . . . . .	13
2.8	Natural rubber with different shape of bulges. . . . .	14
2.9	Testing result of three different types of bulges. (a)Testing results for prims; (b)Testing results for cones; (c)Testing results for cylinders. . .	14
2.10	An Interdigitated-electrode Thin-film Sensor[20] . . . . .	15
2.11	The Parameters of the interdigital electrodes array . . . . .	15
2.12	The Distribution of Triboelectric and Interdigital Sensors on the Vest .	16
2.13	The Signal acquisition Module based on NRF52810 SoC . . . . .	16
2.14	NRF52810 SoC for BLE Communication . . . . .	17
2.15	Bias and amplifier Circuit for Triboelectric Sensors . . . . .	18
2.16	Bias Circuit for Interdigital Sensors . . . . .	19
2.17	Signals of Sensors under 6 different postures . . . . .	20
3.1	The Logo of NUS Medical Care app . . . . .	22
3.2	The Searching UI for Choosing Device to Connect . . . . .	23
3.3	The Visualization of data based on aAInfographics Framework . . . . .	25
3.4	Supported Vector Machine Theory . . . . .	26
3.5	Diagram of a random decision forest . . . . .	27
3.6	Hybride model structure of gradient boosting decision tree . . . . .	28

3.7	An Illustration of XGBoost . . . . .	30
3.8	An Illustration of AdaBoost . . . . .	31
3.9	An Illustration of LightGBM . . . . .	32
3.10	Confusion Matrixes of six models . . . . .	33
3.11	ROC Curve of six models . . . . .	34
3.12	ROC Curve of six models . . . . .	35
3.13	Realtime Posture Recognition on iPhone . . . . .	37
3.14	The Login Web Page . . . . .	38
3.15	The Visualization Web Page . . . . .	39
4.1	The Structure of the Medical Care System . . . . .	40
4.2	The Working Flow of the Medical Care System . . . . .	41

# List of Tables

2.1	Test results of sensors with three types of budges. . . . .	14
3.1	Training parameters of SVM model. . . . .	27
3.2	Training parameters of random forest model. . . . .	28
3.3	Training parameters of GBDT model. . . . .	29
3.4	Training parameters of XGBoost model. . . . .	30
3.5	Training parameters of AdaBoost model. . . . .	31
3.6	Training parameters of LightGBM model. . . . .	32
3.7	A Comparison among six models . . . . .	36

# Chapter 1

## Introduction

### 1.1 Overview

Adolescent Idiopathic Scoliosis (AIS) is a skeletal and muscular disorder of unknown etiology that occurs during preadolescence or before skeletal growth and maturation, mostly in females aged 10 to 18 years[1]. AIS can cause significant physical and psychological damage to the young person, with the most easily detectable and most concerning physical deformities[2]. Therefore, the prevention and treatment of AIS has been the focus of attention of experts and scholars in the field of spinal surgery and spinal rehabilitation.

Surgery is recognized as an effective treatment for AIS, but statistics show that only 1% of patients with AIS require surgical treatment and that surgery can cause limitations in spinal motion. There is a growing interest in rehabilitation and brace therapy for AIS[3].

Bracing has been used in the treatment of AIS since the Middle Ages, and the earliest braces used only simple plates and ladders for correction[4]. The development of computer-aided design/computer-aided manufacturing (CAD/CAM) technology has facilitated the improvement of braces to make them more accurate, comfortable and effective. Brace fabrication has changed from traditional plaster casts to the use of laser scanners combined with CAD/CAM program design. The CAD/CAM technology is superior to traditional methods.

The finished product is lighter and more comfortable, improving patient compliance. 3D printing technology has also been applied to the production of support devices, through the human body rapid 3D modeling of the human body, which saves time in mold taking and is easy to adjust, is becoming increasingly increasingly

## CHAPTER 1. INTRODUCTION

favored by physicians and patients[5, 6].

However, traditional brace therapy has limitation in dynamic evaluation of patient state. Because the visual impact of poor posture is more severe, it is important to assess the trunk imbalance in patients with AIS while developing a rehabilitation program and to design an individualized rehabilitation program for the patient. Traditional 3D printed brace for patient can only restrict the wearer from performing imbalanced and harmful movements and provide a traction to the spine and trunk, but does not have the ability to assess and analyze the patient's posture. In order to better help patients keep track of their health and posture, and to assist doctors in evaluating and diagnosing patient outcomes and providing feedback to patients, the traditional brace needs to be improved in the direction of intelligence[7].

With the development of artificial intelligence and 5G technologies, internet of things (IoT) technology has reached a new level which provides the platform to support the communication of portable devices[8]. Under this circumstance, IoT devices enhanced by artificial intelligence have a wide range of applications in many wearable application scenarios such as healthcare, sports monitoring and human-machine interfaces][9].

However, in the field of wearable devices, power supply has always been a hot issue[10, 11]. The size and mass of wearable devices are relatively small, and it is a challenge to power them for as long as possible without destroying the overall structure of the device.

One solution is to use low-powered or even self-powered components in the wearable device to support the function. Recently, a new type of power-generation device called a triboelectric nanogenerator (TENG) had been developed based on the coupling mechanism between the triboelectric charge and the electrostatic induction for which small-scale mechanical energy is used. Advantages of TENGs include efficiency, low cost, stability, robustness, simplicity in manufacturing, and environmental friendliness. It serves as power generators, but the producing electricity from the mechanical triggering also reveals the potentials for self-powered sensing uses.

Despite the advantage of triboelectric sensors, the coupling mechanism of TENGs limits its capability for recognizing static posture owing to the lack of significant mechanical movement for producing electric signal.

Recently, interdigital electrodes are widely used in acoust sensing area owing to its

## CHAPTER 1. INTRODUCTION

sensitivity to different frequencies. But the interdigital electrode array structure also has the potential to work as pressure sensor. While the pressure exerted increasing, the resistance of the sensor keeps pace with the pressure.

Considering the complex diversity of human postures and movements, it is a challenge to carry out the recognition of human postures through sensors. The traditional threshold-based triggering scheme is difficult to be used to determine similar postures with relatively low accuracy. Additionally, machine learning, as an emerging technology, has strong potential to extract subtle differences and processing multi-channel signals, which is a perfect solution for recognizing different postures and producing medical analysis[12].

### 1.2 Innovation and Motivation

This report proposed an AIoT-enhanced e-vest for assisting adolescent scoliosis patients with correction and enabling real-time recognition of the patient's posture.

In order to give timely feedback to the patient, "NUS Medical Care", a mobile phone software based on the IOS platform, was developed to visualize the wearer's body data in real time. In addition, the software enables real-time posture recognition and transmission of body data to a remote server database called "Firebase", which provides data support for doctors to conduct remote consultations.

For facilitating doctors' analysis of the patient's condition, we developed a cross-platform web page to visualize and analyze the patient's daily posture and movement, and to provide medical feedback to patients.

### 1.3 Report Synopsis

The rest of this report is organized as follows. In chapter 2, we proposed a e-vest design with two kinds of sensors and a signal acquisition communication module. In chapter 3, an app based on iOS platform is introduced for BLE communication and data updating with a cross-platform web page for signal visualization. In chapter 4, we integrate the whole system for testing the completeness and in chapter 5 we draw a conclusion of the project and give a further discussion for the future work.

# Chapter 2

## Front-End Design

### 2.1 E-Vest Design

The brace-based treatment protocol for the correction of adolescent scoliosis has been shown to have a good therapeutic effect. Therefore, in this section, we also propose an e-vest for corrective purposes as well as intelligent analysis based on the principles of brace therapy.

#### 2.1.1 Vest Fabrication

According to the material of the brace, we can classify the brace into soft body and hard body. The design principle of soft brace is mainly based on bioactive feedback mechanism, which does not impede the wearer's movement too much, cut less visible under the clothing and has a higher compliance with the wearer. However, according to the study, we found that for patients with high degree of scoliosis in the rapid growth period, the use of rigid brace can better help patients to control the progress of scoliosis. Therefore, in order to better help patients with scoliosis correction treatment, we use a rigid material support as the basis of the vest design.

In addition, traditional rigid braces have relatively low compliance and are often less comfortable to wear, which can also reduce the effectiveness of orthopedic treatment. The development of computer-aided design and computer-aided manufacturing technology has promoted improvements in the manufacture of braces, making them more accurate, comfortable, and effective. While traditional braces are often made by plaster casts, the combination of laser scanners and CAD/CAM technology allows us to create lightweight, comfortable braces that are more compliant to patients.

## CHAPTER 2. FRONT-END DESIGN

In addition, the development of 3D printing technology provides a new way of manufacturing braces. Rapid 3D modeling of the human body through laser scanning technology is a good solution for the manufacture of braces, as it saves time in acquiring the model and facilitates minor adjustments at a later stage.

Therefore, for the production of the vest in this report, we used 3D printing technology combined with laser scanner-based 3D modeling technology for the vest. In terms of material, we chose polyethylene as the main material for the vest matrix. Because polyethylene has good thermoplasticity, it is suitable for 3D printing technology and can fit the wearer's body very well. Moreover, polyethylene is relatively hard and can be used as a rigid material to provide strong support to help patients with scoliosis correction.

## 2.2 Sensor Fabrication

By integrating sensors into the 3D printed polyethylene orthopedic vest, real-time monitoring of human posture is possible. By integrating sensors into the 3D printed polyethylene orthopedic vest, real-time monitoring of human posture is possible. By analyzing the human posture, we can classify the posture into dynamic and static. Dynamic postures include all movement patterns such as walking, running, jumping, etc., while static postures include those with little or no movement, such as standing, sitting, lying, etc.

### 2.2.1 Triboelectric Sensor

For dynamic posture recognition, inertial sensors are often a good solution to determine the type of posture by calculating the acceleration of the motion. However, inertial sensors are active sensors that require an external power supply, which is not conducive to long-time operation for wearable devices with limited energy storage.

The newly proposed triboelectric generator is a perfect solution to detect dynamic motion. The primary working principle of TENG is based on the triboelectrification and electrostatic induction effects. In this project report, six-layer textile-based triboelectric sensors under CS operation mode are proposed. Moreover, the following experiments are all based on these sensors.

### 2.2.1.1 Theory of TENG

Triboelectrification is a common nature effect that has been observed in human's early days. However, it is always treated as an adverse effect in traditional applications, for example, electronics, gas transportation, etc. [13]

Triboelectric nanogenerator (TENG), which was first put forward by Wang's group, has opened up a new era for utilizing the ignored and uncontrollable energy in triboelectrification. The working theory of TENG is mainly based on the coupling of contact electrification and electrostatic induction. Taking the contact-separation (CS) mode as an example, when two polymer films with different electron-attracting capabilities contact and separate, the tribocharges caused by contact electrification will induce an electrical potential difference in the interfacial region and back electrodes, leading to the current flow if there is external load.

### 2.2.1.2 Four Basic Working Modes of TENG

An effective mechanical-to-electrical conversion mechanism has witnessed remarkable progress and numerous successful applications as both power sources and self-powered sensors. With the rapid growth in this field, the systematic framework of TENG has been built up, including the basic working modes, theoretical equivalent model, structures, the friction materials, and the figure of merit. Apart from the contact-separate mode, there are three other working modes of TENG, i.e., the linear-sliding mode, the single electrode mode, and the freestanding triboelectric-layer mode.

W. Ding et al.,[14] summarized the pros and cons for the four basic working modes from both the energy harvesting and sensing perspectives, as provided in Figure 2.1. In practice, each mode has its unique characteristics and superiority, which should be appropriately chosen or jointly used for specific applications.

### 2.2.1.3 Basic Theory of TENG

In 1861, based on Gauss's theorem, ampere's law, Faraday's electromagnetic law and other equations, Maxwell creatively introduced displacement current into it and predicted the existence of electromagnetic wavelengths. Maxwell's system of equations is shown below:

## CHAPTER 2. FRONT-END DESIGN

Working mode	Contact-separation mode	Linear-sliding mode	Single electrode mode	Freestanding triboelectric-layer mode
Schematic				
Pros	<ul style="list-style-type: none"> <li>1. Simple structure, great robustness, high instantaneous power density</li> <li>2. Easy to fabricate, model and analyze.</li> </ul>	<ul style="list-style-type: none"> <li>1. Generate triboelectric charges more effectively than the pure contact, with a greatly enhanced output power.</li> <li>2. Easy to involve advanced design for high-performance TENGs, for example, grating structure.</li> <li>3. Can be made into fully packaged form and operate in vacuum.</li> </ul>	<ul style="list-style-type: none"> <li>1. Only require one electrode to work, which reduces the system restriction as well as complexity and increases the flexibility.</li> </ul>	<ul style="list-style-type: none"> <li>1. There can be no direct physical contact between the two triboelectric layers, which will cause no material abrasion and heat generation.</li> <li>2. Can harvest the energy from a moving object but with the entire system mobile without grounding.</li> </ul>
Cons	<ul style="list-style-type: none"> <li>1. Require a volume varying cavity design, leading to a challenge for packaging</li> </ul>	<ul style="list-style-type: none"> <li>1. Frequency friction may cause significant wear and tear, which reduces the durability and robustness.</li> </ul>	<ul style="list-style-type: none"> <li>1. The electron transfer is not effective due to the electrostatic screening effect, which results in a lower output performance</li> </ul>	<ul style="list-style-type: none"> <li>1. The small gap between the two electrodes can cause severe electric discharging and lead to air breakdown.</li> </ul>

Figure 2.1: The summarization of four basic working modes of TENG.

$$\nabla \cdot \mathbf{D} = \rho_f \quad (\text{Gauss's Law}) \quad (2.1)$$

$$\nabla \cdot \mathbf{B} = 0 \quad (\text{Gauss's Law of Magnetism}) \quad (2.2)$$

$$\nabla \cdot \mathbf{E} = -\frac{\partial \mathbf{B}}{\partial t} \quad (\text{Faraday's Law}) \quad (2.3)$$

$$\nabla \cdot \mathbf{H} = \mathbf{J}_f + \frac{\partial \mathbf{D}}{\partial t} \quad (\text{Maxwell-Ampere's Law}) \quad (2.4)$$

where  $D$  is the displacement field, which can be expressed as  $D = \epsilon_0 E + P$ ;  $\rho_f$  is the free charge density,  $B$  is the magnetic field,  $E$  is the electric field,  $H$  is the magnetization field,  $J_f$  and  $D$  is the free current density.

The second term in Equation 2.4 is defined as Maxwell displacement currents, which can be expressed as:

$$J_D = \frac{\partial D}{\partial t} = \epsilon_0 \frac{\partial E}{\partial t} + \frac{\partial P}{\partial t} \quad (2.5)$$

For many subsequent years, researchers have mostly combined the first and second terms of Maxwell's displacement current to obtain the following equation:

$$J_D = \epsilon \frac{\partial E}{\partial t} \quad (2.6)$$

However, Equation 2.6 is only applicable to the general homogeneous media. When considering a medium with surface polarization charge such as friction material, the contribution of polarization density  $P_s$  caused by surface electrostatic charge is not negligible in the set of equations for displacement current, as shown in the following expressions:

$$J_D = \frac{\partial D}{\partial t} = \varepsilon \frac{\partial E}{\partial t} + \frac{\partial P_s}{\partial t} \quad (2.7)$$

The first term in Equation 2.7 is the current due to the change of electric field, which unifies the electric and magnetic fields and provides strong theoretical brace for technologies related to electromagnetic waves such as radio, radar and wireless communication. The second term in the equation is the current caused by the corresponding polarization field due to the presence of electrostatic charges on the surface. It is the theoretical source of the triboelectric nanogenerator, which provides the theoretical basis for the application of triboelectric nanogenerators in energy and sensing fields.

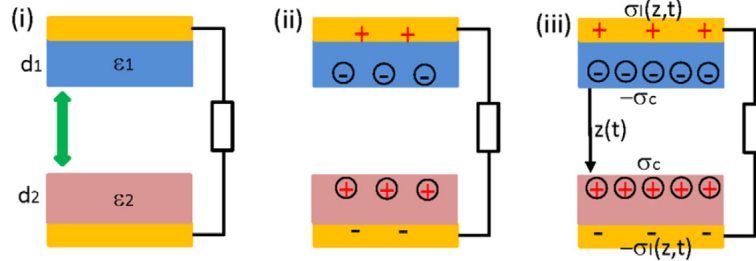


Figure 2.2: Fundamental principle of TENG.

Taking the vertical contact-separated friction nanogenerator as an example, we will explain its basic theory in detail[15]. As shown in Figure 2.2a, in a vertical contact-separated friction nanogenerator, the dielectric constants of two friction materials are  $\varepsilon_1$  and  $\varepsilon_2$ , and their thicknesses are  $d_1$  and  $d_2$ . When two friction materials are in contact, the frictional charging effect causes the electrostatic charge to be transferred to the surfaces of the two materials. As the number of contacts increases, the charge density  $\sigma_c(t)$  on the surface of the two friction materials will increase until saturation is reached (Figure 2.2b); in the process of contact separation, due to the potential difference between the two electrode materials, electrons will be

transferred between the two electrodes, the amount of charge transferred is  $\sigma_1(z, t)$ , which is expressed as a function of the distance between the two friction materials  $z(t)$ . As shown in Figure 2-4c, the electric field built in the two friction materials is  $E_Z = [\sigma_t(z, t)/\varepsilon_1]$  and  $E_Z = [\sigma_t(z, t)/\varepsilon_2]$  respectively, while the electric field in the gap between the two separated materials is  $E = [\sigma_l(z, t) - \sigma_c]/\varepsilon_0$ , so the induced potential difference between the two electrodes is:

$$V = \sigma_1(z, t) [d_1/\varepsilon_1 + d_2/\varepsilon_2] + z [\sigma_1(z, t) - \sigma_c]/\varepsilon_0 \quad (2.8)$$

In the case of short circuit, i.e.  $V = 0$ , the power flowing through the two electrodes can be expressed as:

$$\sigma_I(z, t) = \frac{z\sigma}{d_1\varepsilon_0/\varepsilon_1 + d_2\varepsilon_0/\varepsilon_2 + z} \quad (2.9)$$

As a result, the displacement current can be denoted as:

$$J_D = \frac{\partial D_z}{\partial t} = \frac{\partial \sigma_l(z, t)}{\partial t} \quad (2.10)$$

$$= \sigma_C \frac{dz}{dt} \frac{d_1\varepsilon_0/\varepsilon_1 + d_2\varepsilon_0/\varepsilon_2}{[d_1\varepsilon_0/\varepsilon_1 + d_2\varepsilon_0/\varepsilon_1 + z]^2} + \frac{d\sigma_C}{dt} \frac{z}{d_1\varepsilon_0/\varepsilon_1 + d_2\varepsilon_0/\varepsilon_1 + z} \quad (2.11)$$

When the triboelectric nanogenerator is connected to an external load  $R$ , the output current of the triboelectric nanogenerator can be expressed as following equation according to Ohm's law,  $U = IR$ :

$$RA \frac{d\sigma_l(z, t)}{dt} = z\sigma_c/\varepsilon_0 - \sigma_I(z, t) [d_1/\varepsilon_1 + d_2/\varepsilon_2 + z/\varepsilon_0] \quad (2.12)$$

#### 2.2.1.4 TENG Materials

When two different materials come in contact, one of them loses electrons, and the other gains electrons due to the difference in their electronegativity contact-induced electrification named triboelectricity.

Since the triboelectric effect exists in almost all materials, including metals, polymers Figure 2.3 summarizes the triboelectric series of a series of everyday materials.[16] The arrow pointing upward indicates the more robust ability to lose electrons, and the arrow pointing down suggests the more robust ability to gain electrons. Ideally, the usage of two materials with large differences in the ability to gain and lose electrons can increase the triboelectric effect and obtain a higher charge transfer rate.

Material name	Affinity nC/J	Material name	Affinity nC/J
Polyurethane foam	+60	PET (mylar) cloth	-40
Sorbothane	+58	EVA rubber	-55
Box sealing tape (BOPP)	+55	Gum rubber	-60
Hair, oily skin	+45	Hot melt glue	-62
Solid polyurethane, filled	+40	Polystyrene	-70
Magnesium fluoride (MgF2)	+35	Nickel, Copper	
Nylon, dry skin	+30	Polyimide	-70
Machine oil	+29	Silicones	-72
Nylatron (nylon filled with MoS2)	+28	Vinyl: flexible	-75
Glass (soda)	+25	Carton-sealing tape (BOPP)	-85
Aluminum		Olefins: LDPE, HDPE, PP	-90
Paper (uncoated copy)	+10	Cellulose nitrate	-93
Wood (pine)	+7	Office tape backing	-95
GE brand Silicone II	+6	UHMWPE	-95
Cotton	+5	Neoprene (polychloroprene)	-98
Nitrile rubber	+3	PVC (rigid vinyl)	-100
Wool	0	Latex (natural) rubber	-105
Steel		Viton, filled	-117
Polycarbonate	-5	Epichlorohydrin rubber, filled	-118
ABS	-5	Santoprene rubber	-120
Acrylic (polymethyl methacrylate)	-10	Hypalon rubber, filled	-130
Epoxy (circuit board)	-32	Butyl rubber, filled	-135
Styrene-butadiene rubber	-35	EDPM rubber, filled	-140
Solvent-based spray paints	-38	Teflon	-190

Figure 2.3: Triboelectric series for some commonly materials following a tendency of easy losing electrons (positive) to gaining electrons (negative).

### 2.2.1.5 Structure of Triboelectric Sensor

The primary working principle of TENG is based on the triboelectrification and electrostatic induction effects. The glovework sensors in the first and second mode because of the hand's motion usually bring a quick contact and a slight linear slide. The former will generate high instantaneous power, which can be collected as a signal of the sensor. In this project report, six-layer textile-based triboelectric sensors under CS mode are proposed. Furthermore, the following experiments are all based on these sensors.[17]

The sensor's top and bottom layers are soft cotton textiles, which are used to isolate the skin and protect the sensor-sensing part. The two layers just adjacent

## CHAPTER 2. FRONT-END DESIGN

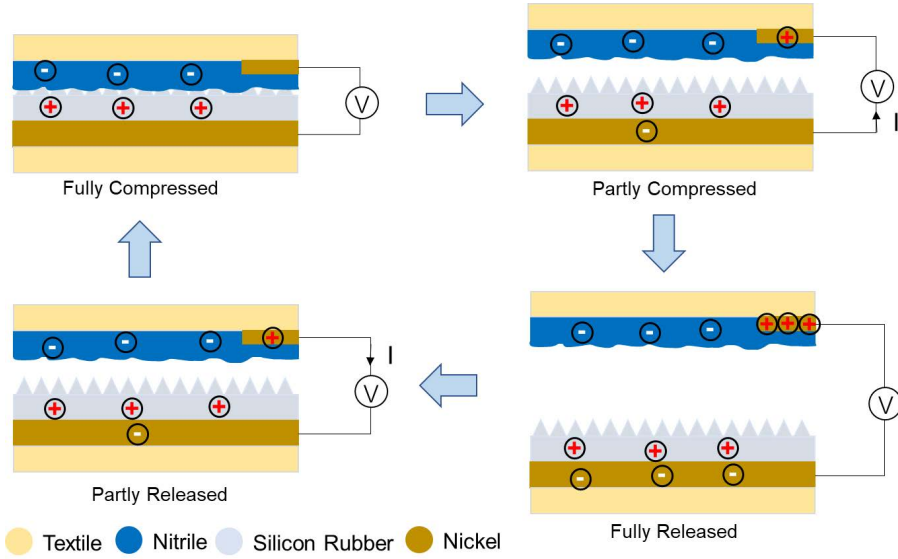


Figure 2.4: Working process of TENG under CS operation mode.

to the upper and lower surface layers are made of nickel, which is used to collect electrons and transmit the functional layer's signals to the processing circuit through wires. The innermost two layers are functional, consisting of nitrile and silicon rubber, used to realize the triboelectric mechanism based on CS mode.

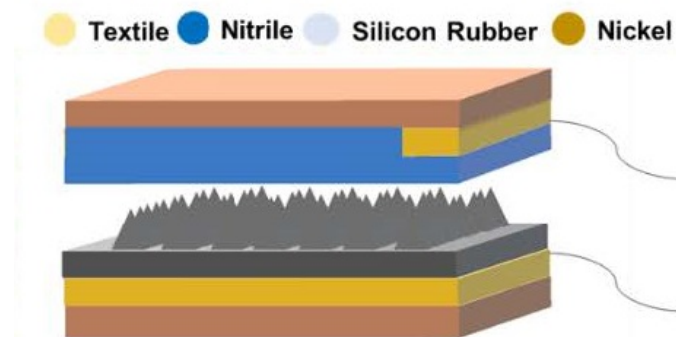


Figure 2.5: 3D structure of the triboelectric sensor.

as two dissimilar materials, when nitrile and silicon rubber are brought into contact, electrons are transferred from silicon rubber's contact surface to nitrile due to the difference in electron affinity. Thus, the two contact surfaces are equipped with equal but opposite charges after separation. During working, the established

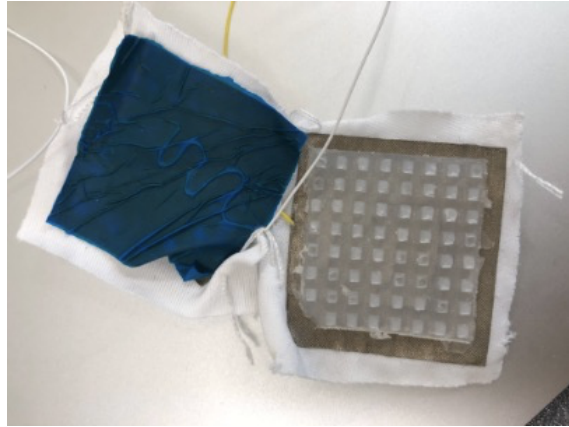


Figure 2.6: A picture of the real triboelectric sensor

and disappeared electric potential difference will drive electrons to flow back and forth in the external circuit, thus generating electrical energy.

#### 2.2.1.6 Fabrication of Triboelectric Sensor

The triboelectric textile sensor contains two layers: a positive charge generation layer and a negative charge generation layer. Firstly, the conductive textile is cut into the desired size and shape, made of metallized fabric (polyester Cu) coated with an adhesive. A thin nitrile film is attached to one side of a conductive textile to fabricate the positive charge generation layer.[18]

Another conductive textile is coated with silicone rubber film on one side as well. The coating process was firstly dispensing required amounts of parts a and B of the *EcoFlex<sup>TM</sup>* 00-30 into a mixing container (1A:1B by volume or weight), followed by mixing the blend thoroughly for 3 min, and then the mixed solution was poured into a 3D-printed mold followed by 2 hour baking at 50 °C for curing after using vacuum dryer to eliminate the bubble in the mixture.

For the textile sensor without surface structures, the uncured mixture was directly pasted onto the conductive textile to form a flat surface. Lastly, the silicone rubber-coated textile was stitched to the nitrile-coated textile with two nonconductive textiles attached to the outer sides for encapsulation; the detailed fabrication sees the Supplementary Information.



Figure 2.7: 3D-printed molds for EcoFlex

#### 2.2.1.7 Surface Feature

To strengthen the sensors' output signal, specially designed bulges are added to the surface of the textile layers. To test the budge shape with the best performance, three typical shapes of budges with spacing distance at  $2.00\text{ mm}$  are fabricated on the surface of *EcoFlex<sup>TM</sup>* layer after molding.

While exerting the same force with fixed bending speed to a sensor, use an oscilloscope to test sensor output analog signal after preprocessed. The result is as shown in Figure 2.8.

As the testing result indicates, the sensor with cone shape budges has the highest output considerable peak-to-peak value when exerting the same force. The advanced performance of surface design provides a platform to convey the signal of the slightest gesture. Additionally, the higher output level raises the signal-to-noise ratio (SNR), strengthening the system's stability.

#### 2.2.2 Interdigitated Sensor

Despite triboelectric sensor has great potential to detect dynamic posture, some static posture cannot be recognized accurately owing to the lack of features. To enhance e-vest's ability to recognize static posture, relying on triboelectric sensors

## CHAPTER 2. FRONT-END DESIGN

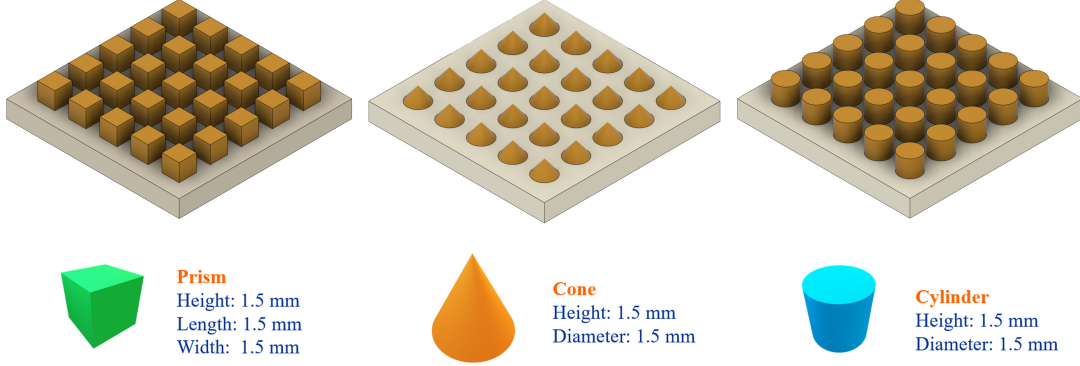


Figure 2.8: Natural rubber with different shape of bulges.

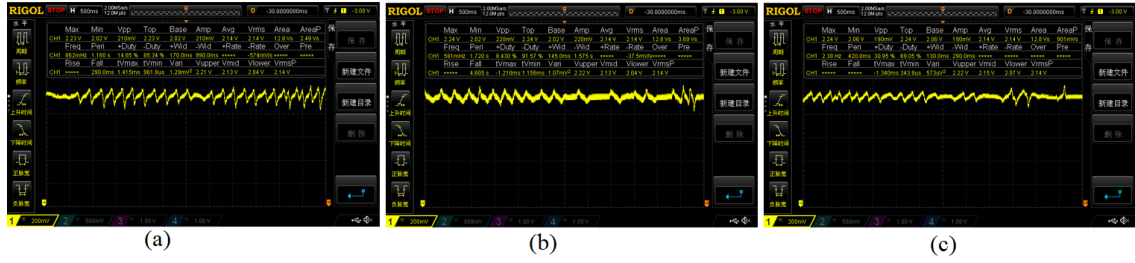


Figure 2.9: Testing result of three different types of bulges. (a)Testing results for prims; (b)Testing results for cones; (c)Testing results for cylinders.

Table 2.1: Test results of sensors with three types of bulges.

	Prism	Cone	Cylinder
$V_{rms}$	2.14V	2.14V	2.14V
$Top$	2.23V	2.24V	2.24V
$Base$	2.02V	2.02V	2.06V
$V_{pp}$	210mV	220mV	190mV

alone may have limited effect. Therefore, in this report, we use an interdigital-electrode resistive sensor to enhance the recognition of static poses.

According to Prof. Lakin's discovery[19], interdigital electrode has resistance effects. Interdigitated-electrode arrays are widely used in surface acoustic wave and other fields due to their miniaturization and high signal-to-noise ratio. Besides, interdigital electrode array has the capability to work as a mechanical pressure sensor to detect the contact between e-vest and wearer's body.

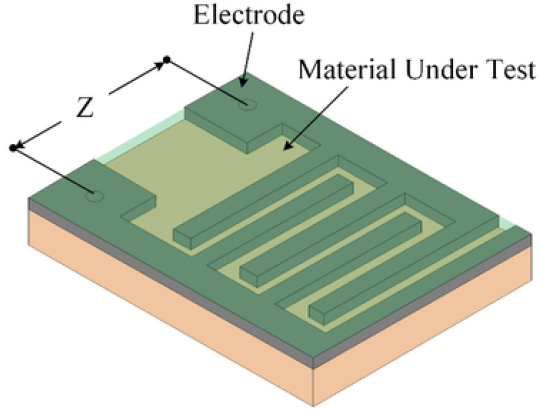


Figure 2.10: An Interdigitated-electrode Thin-film Sensor[20]

Figure 2.10 illustrates an interdigitated-electrode thin-film sensor mounted on a semiconductor composite material carrier. By applying a force to the sensor, the contact area between the electrodes and the semiconductor layer can be increased, thereby reducing the resistance between the two electrodes. The parameter of electrodes is shown in Figure 2.11

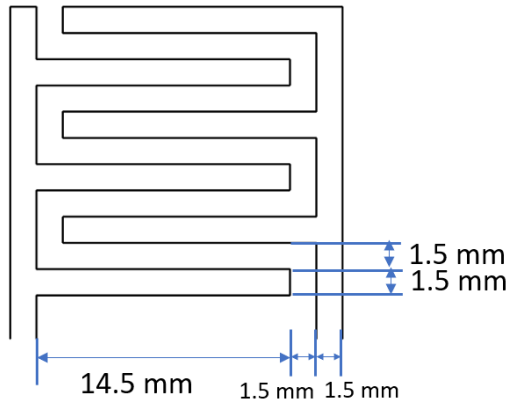


Figure 2.11: The Parameters of the interdigital electrodes array

### 2.2.3 Distribution on Vest

In the design of the vest, we adopt five triboelectric sensors for detecting dynamic motions of body and five interdigital sensors for sensing static postures. The distribution of sensors on the vest is shown in Figure 2.12. Each five sensors are respectively placed on the chest, lower back, upper back, armpit, and waist. These

five positions are sensitive to the motions of limbs, the trunk and waist, which can cover most of movements of patients.



Figure 2.12: The Distribution of Triboelectric and Interdigital Sensors on the Vest

## 2.3 Signal Acquisition Module

The previous section introduced the sensing solution in the design of e-vest. To collect the signal from sensors and achieve aIoT application in this system, we should build a signal acquisition module.

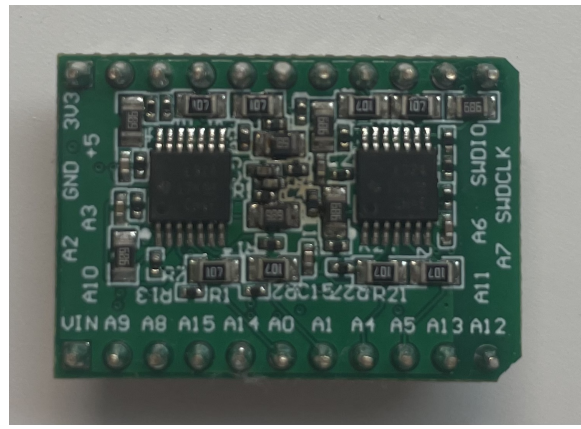


Figure 2.13: The Signal acquisition Module based on NRF52810 SoC

### 2.3.1 BLE Communication

Reducing power consumption is a key in this project. Therefore, choosing the appropriate communication method helps to reduce the power consumption of the system. In addition, the size of the circuit module should be as small as possible due to the demand of wearable.

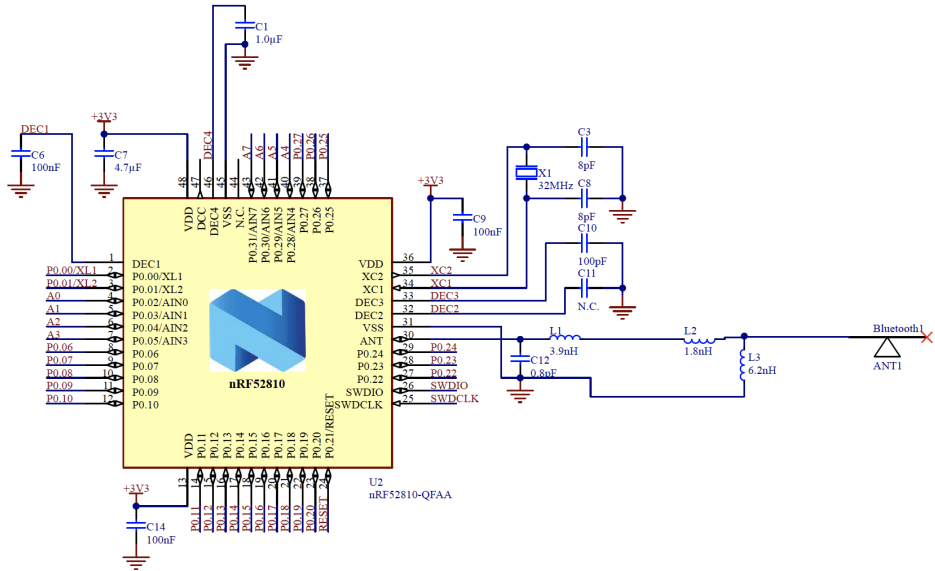


Figure 2.14: NRF52810 SoC for BLE Communication

In this project, we adopt NRF52810 Soc from Nordic Semiconductor as the MCU of the signal acquisition module. NRF52810 Soc integrates various communication protocols suitable for low-power Bluetooth and 2.4GHz ultra-low-power wireless applications.

### 2.3.2 Analog-Digital Convert

Since the signal generated by the triboelectric sensor is an aC signal, a single power supply is used in the circuit design. In a single power supply system, the negative half of the aC signal will be clipped. In order to fully obtain the characteristics of the triboelectric sensor signal, a voltage divider composed of two resistors R1 and R2 are required to provide the DC conversion voltage.

Since the triboelectric sensor has a high output converter, it is usually in the  $M\Omega$  level, so the resistance in the voltage divider circuit should be replaced with a

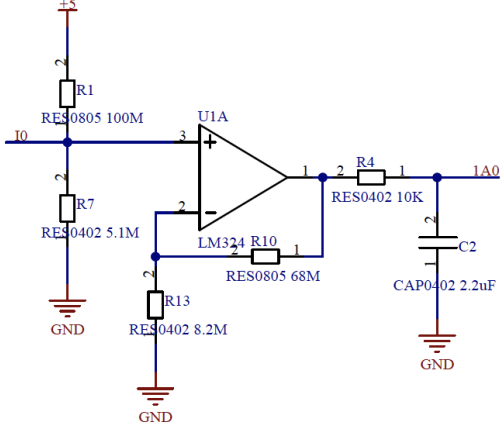


Figure 2.15: Bias and amplifier Circuit for Triboelectric Sensors

large one, and it should also be designed in the  $M\Omega$  level to provide a high input signal processing circuit impedance. The average voltage after bias is at 242.5 mV. The incremental voltage calculation formula is as follows:

$$V_{\text{Bias}} = V_{\text{CC}} \times \frac{R_7}{R_1 + R_7} \quad (2.13)$$

AC-coupled non-inverting amplifier LM324 is used to amplify or follow the aC signal output from the bias circuit. The gain can be calculated and adjusted through resistors R10 and R13. However, since the actual output voltage signal amplitude of LM324 is 3.5V, if the amplification factor is too large, making the output signal more remarkable than the upper threshold, there will be an error between the actual value of the amplification gain and the theoretical value. In addition, since the maximum output voltage of 3.5V does not exceed the aDC input range of arduino, overvoltage protection is not required. In this design, given that the triboelectric sensor's output signal is large enough, R13 is chosen to be much larger than R5 to obtain the effect of a voltage follower. The calculation formula of gain  $G$  is as follows:

$$G = 1 + \frac{R_{10}}{R_{13}} \quad (2.14)$$

For detecting the signal from interdigital sensors, we should use partial voltage method to convert the analog signal to digital signal with a BL1551 chip to work as an analog switch shown in Figure 2.16.

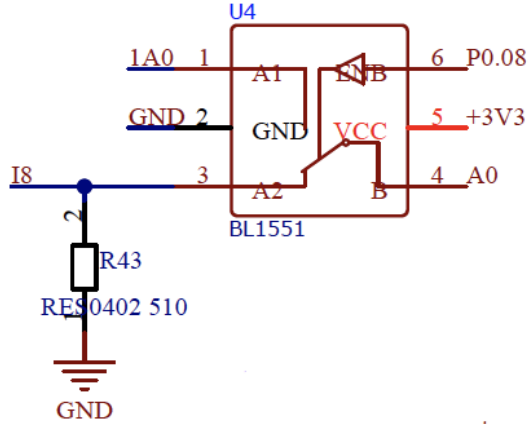


Figure 2.16: Bias Circuit for Interdigital Sensors

## 2.4 Establishment of Data Set

For training a machine learning model to recognize different gestures, enough valid data set is the base requirement. In this stage, a python program communication with signal acquisition module is built up through BLE. During the process of communication, the sensors on the vest provides ten channels of signals, while the program will extract 200 sampling points of each channel and pack them up as a batch. The operator should repeat the same gesture over 250 times to support building up a adequate model.

In this part, the data of sensors under six specific postures are collected, and each posture is executed in 200 consecutive groups, and each group is sampled 200 times from ten sensor channels for machine learning model training.

In Python, the program collects the sampled value of the sensors signal via BLE. Since the original data is a time series, preprocessing is required to convert the time data series into data segments. A data group is saved in an Excel file in the form of a column. The length of a column is  $10 \times 200 = 2000$ , and there are  $6 \times 250 = 1500$  batches of gesture data in total. Then, the entire data set is randomly divided into a training set (1200 data sets) and a test set (300 data sets).

## CHAPTER 2. FRONT-END DESIGN

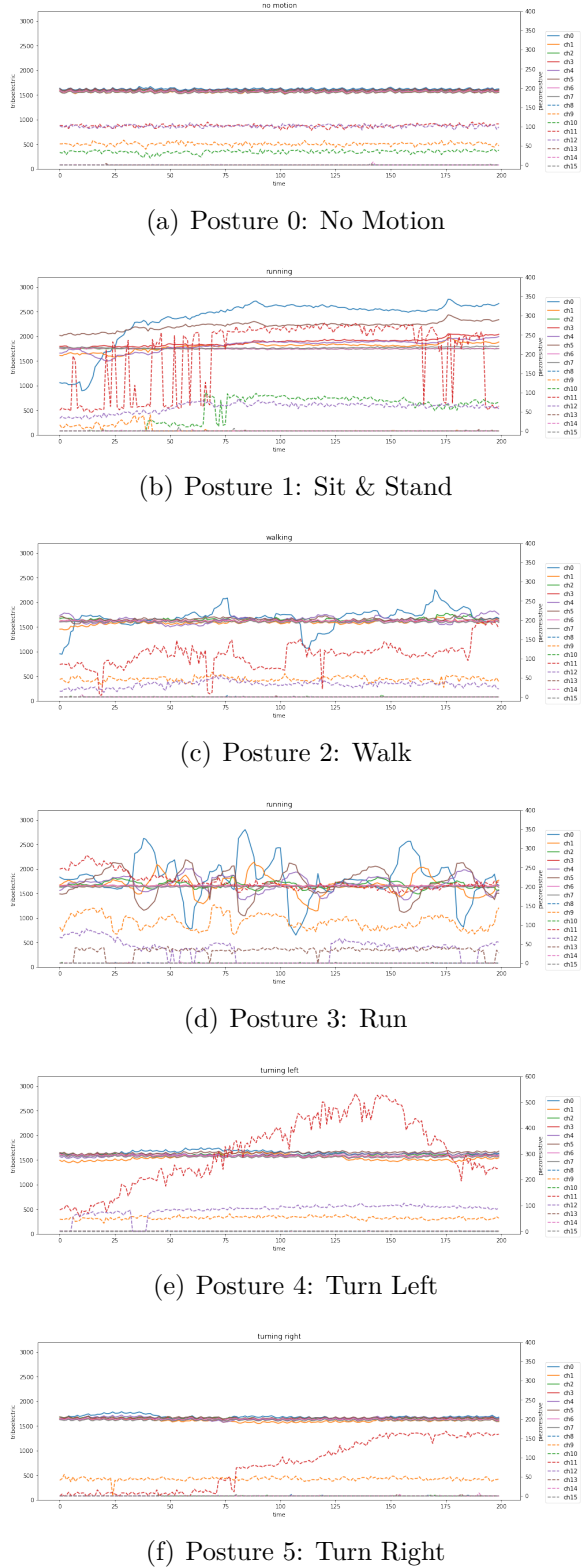


Figure 2.17: Signals of Sensors under 6 different postures

# Chapter 3

## Back-End Design

### 3.1 App on phone

For collecting the data from signal acquisition module via BLE, we should use devices with networking capability. Considering the standby time of the device and its portability, we decided to use the cell phone as the medium of signal transmission. In modern society, cell phones have become an essential device for human beings to support their daily needs for calls, communication, and entertainment. The addition of cell phones allows the system to move away from traditional computer-based wireless transmission solutions, making the undershirt smarter and more convenient to wear and use, without being limited to whether or not you have the environment to use a computer.

At present, cell phone people are in a stage of rapid development, users' requirements for the functions and performance of cell phone devices are getting higher and higher, at the same time, cell phone application software pages are gradually used in all walks of life. At this stage, there are mainly two mainstream application platforms for smart phones, which are the iOS system developed by apple and the android system provided by Google, etc.

Considering the smoothness of the operating experience, the stability of the system, the clean design line and other aspects, iOS operating system has a greater advantage, and aPP Store also brings iOS unparalleled advantages of other systems. It integrates applications developed based on iOS, which protects the interests of program developers on the one body and facilitates the retrieval of applications by system users on the other. Based on these advantages, more and more industries are choosing iOS to develop applications to serve their users. At the same time, the

closed nature of iOS system can also bring more security assurance. The health information of the patients involved in this project is also sensitive and needs to be prevented from being stolen by hackers. By analyzing these features of iOS, we chose to develop the application based on iOS platform in this report.



Figure 3.1: The Logo of NUS Medical Care app

In this report, we developed an app based on IOS platform where we implemented three functions in the app: BLE connection, visualization, machine learning and updating.

### 3.1.1 BLE Connection

Bluetooth Low Energy (BLE) is a wireless personal area network technology designed and marketed by the Bluetooth SIG for novel applications in the medical, fitness, beaconing, security and home entertainment industries. Compared to Classic Bluetooth, Bluetooth Low Energy is designed to significantly reduce power consumption and cost while maintaining similar communication range.

Since BLE is a wireless communication, its communication medium is a frequency band resource in a certain frequency range; BLE is marketed for individual and residential use, so it uses the free ISM band (frequency range is 2.400-2.4835 GHz); in order to support multiple devices at the same time, the entire band is divided into 40 parts, each with a bandwidth of 2 MHz, called RF Channel.

The central device manages multiple connected peripheral devices, and the peripheral devices can only connect to one central device. In this application, the e-vest works as the peripheral device and the iPhone device work as the central device.

## CHAPTER 3. BACK-END DESIGN

Before using the function for supporting the e-vest, we should build the BLE connection between iPhone and e-Vest. BLE devices discover other devices over a broadcast channel, with one device broadcasting while the other device scans. Thus, we design a user interface in the app for user to find the broadcast from the e-vest. Once the user tap the correct broadcast in Figure 3.2, the app will check whether the UUID of the device satisfy the requirement. If the UUID of the device is in the permitted list, the BLE connection is built up successfully.

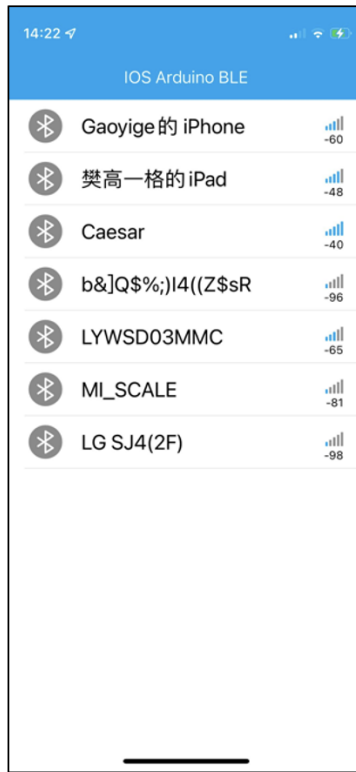


Figure 3.2: The Searching UI for Choosing Device to Connect

In this application, the NRF25810 SoC sends data through Universal asynchronous Receiver/Transmitter (UART) technique. Thus, if we want to receive data from or send data to the vest, we should use the service characteristics UUID to support the function.

Once we receive the data from e-vest, we first need to decode and process the data. The data transfer via UART is based on hexadecimal byte code, so to restore to get the original data, we first restore the data to decimal data. In the BLE bytecode, we convert each decimal data into 2 bytes of hexadecimal number and

stitch them together for transmission. Therefore, we also need to split the received data by every two bytes and do the decoding work.

After connected, we create a text window for observing the data in real time. For each group data, we automatically add the timestamp at the head and plot the data in the text window. Based on the difference in the speed at which Bluetooth sends data, the phone will receive roughly 30 to 50 sets of data per second. Therefore, we also enable live scrolling in this window to ensure that the latest data received is displayed at the top.

### 3.1.2 Visualization

Limited by the capacity of the phone's memory, we cannot store all the accepted data and visualize them all indefinitely, so we need to create a visualization window to limit the length of the instantly stored data.

Moreover, the traditional array-based data storage is not suitable for the case of limited data length, and we cannot directly discard the data at the head of the array or directly insert new data at the end due to the underlying design of the data structure, so we need to design a new container to store the data.

According to the visualization requirements, we need to keep the latest data in a length-defined window in real time. We design a ring storage container with fixed length based on the design idea of RingBuffer, which is based on an array. There are two indexes in the container, one of which is fixed at the initial starting point of the array in the container, and the other index is gradually moved back with new data updates until it reaches the end of the array and then automatically returns to the head of the array, forming a closed ring container. For visualization of the data, we provide a method in the container to return a length fixed array for plotting.

In this app, we implemented the visualization function based on *AAInfographics* framework in Figure 3.3. AAInfographics is the swift language version of aAChartKit which is object-oriented, a set of easy-to-use, extremely elegant graphics drawing controls, based on the popular open source front-end chart library Highcharts. It makes it very fast to add interactive charts to the mobile projects. It supports single touch-drag for data inspection, multi-touch for zooming, and advanced responsiveness for the apps. With the aid of framework, we implemented a multi-channel real time

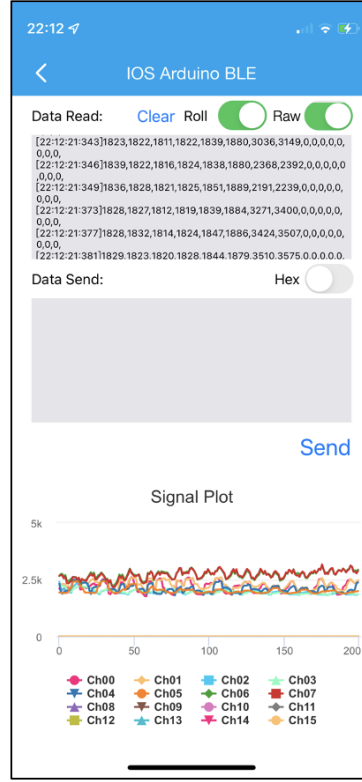


Figure 3.3: The Visualization of data based on aAInfographics Framework

visualization of data.

## 3.2 Machine Learning

In Chapter 2, we have introduced two types of sensors. After analyzing, we know that we can detect the contact between body and sensors by monitoring the amplitudes of the signals. However, there are some disadvantages to judging the amplitudes directly. Firstly, due to the high sensitivity of TENGs to mechanical triggers, slight movements of each finger can be recorded with time information. It will disturb the judgment of the postures. Besides, the ambient environment will affect the signals generated by sensors, which are influenced by temperature, moisture, etc. These external factors increase the instability of the output signals.

Furthermore, the voltage baseline used to determine whether or not a contact is made is always changing as the circuits and sensors are reused. More importantly, each sensor has a different baseline due to manufacturing errors.

In a word, the process of body' movements is quick and complicated. The continuous signal flow associated with the postures has only a few parts, and the unrelated dominant parts mostly correspond to zero activity. One posture is a combination of several basic consecutive movements of each finger. It means that it is necessary to recognize the posture with multi-channel signals in an instant. In order to eliminate instability and realize fast and accurate recognition, several machine learning architecture is built for extract features and recognize postures based on the sensors' signals.

In this section, we trained six different machine learning models to recognize six different postures and conveyed a comparison between these models. After comparison, we implemented the model with the best performance in the iOS app for achieving real time posture recognition.

### 3.2.1 Supported Vector Machine

Support vector machines (SVMs) are binary classification models whose basic model is a linear classifier defined by maximizing the interval on the feature space, i.e. maximum marginal hyperplane (MMH), which distinguishes it from a perceptron; SVMs also include kernel tricks, which make them essentially nonlinear classifiers.??

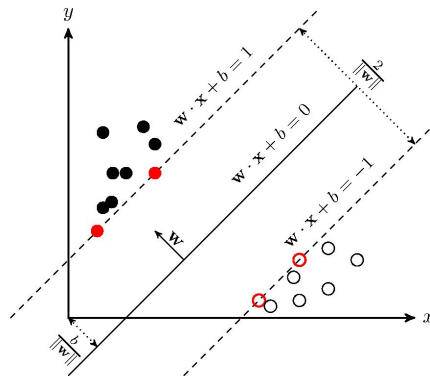


Figure 3.4: Supported Vector Machine Theory

For training the SVM model, the eight-type posture data set is inputted. The parameter of the SVM model is listed in Table 3.1.

Table 3.1: Training parameters of SVM model.

Parameter	Definition	Value/Type
scaler	The scaler of normalize the data set	StandardScaler()
C	The parameter of the tolerance for error	1
loss	a method for evaluating the effectiveness of an algorithm in modeling a data set	hinge

### 3.2.2 Random Forest

A random forest is a classifier with multiple decision trees, and the output class is determined by the plurality of the output classes of the individual trees. In fact, to explain it intuitively, each decision tree is a classifier (assuming that we are now targeting a classification problem), so for one input sample, N trees will have N classification results. And the random forest integrates all the classification voting results and designates the category with the highest number of votes as the final output, which is one of the simplest Bagging ideas. The process of the random forest algorithm is as follows.

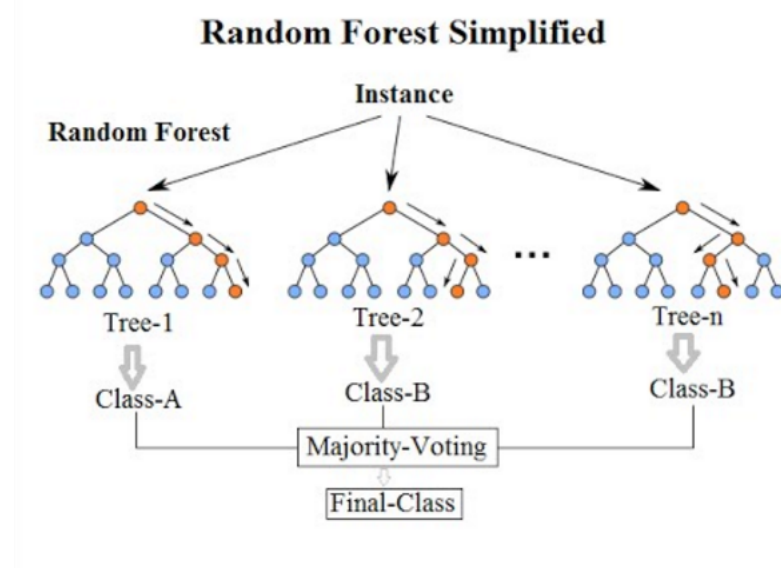


Figure 3.5: Diagram of a random decision forest

The parameters of random forest model is listed in Table 3.2.

Table 3.2: Training parameters of random forest model.

Parameter	Definition	Value/Type
random_state	The seed of random number	0
n_estimators	The number of trees in random forest	1000
max_depth	The maximum depth of trees' division	5
n-jobs	The number of cores to work	4
class_weight	a parameter to adjust the weight of all categories in the sample unbalanced data set	balanced

### 3.2.3 Gradient Boosting Decision Tree

Gradient Boosting Decision Tree (GBDT), also known as MART (Multiple additive Regression Tree), is an iterative decision tree algorithm, which consists of multiple decision trees, and the conclusions of all trees are accumulated to make the final answer.[21] It is considered to be an algorithm with strong generalization ability together with SVM when it was first proposed. In recent years, it has attracted much attention because it is used as a machine learning model for search and sorting. Single decision tree is easy to overfit, but we can suppress the complexity of decision

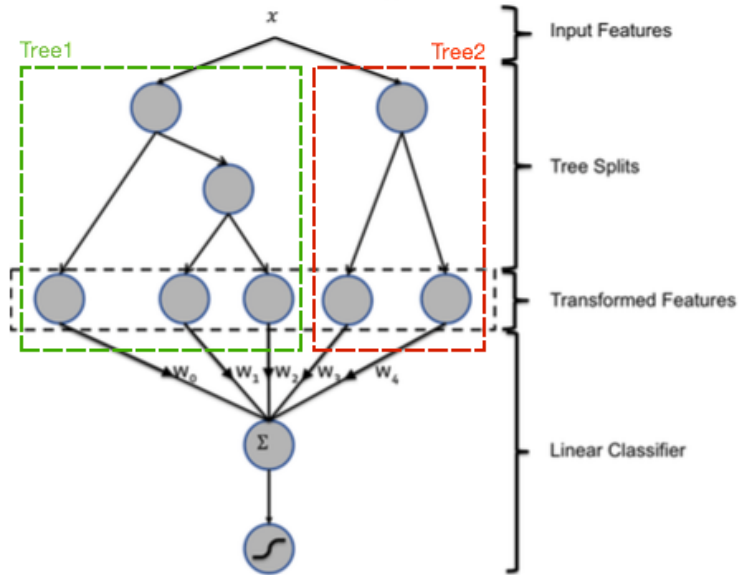


Figure 3.6: Hybrid model structure of gradient boosting decision tree

tree and reduce the fitting ability of single decision tree by various methods, and then integrate multiple decision trees by other means, which can eventually solve

the overfitting problem well.

The core of GBDT is to accumulate the results of all trees as the final result, while there is obviously no way to accumulate the results of classification trees.[22] Boosting is a family of algorithms that can boost weak learners into strong learners, and belongs to the category of ensemble learning.

The parameter of the GDDT model is listed in Table 3.3.

Table 3.3: Training parameters of GBDT model.

Parameter	Definition	Value/Type
random_state	The seed of random number	0
n_estimators	The number of trees in decision tree	100
learning_rate	a tuning parameter that determines the step size of each iteration	0.1
subsample	The number of cores to work	8.00E-01

### 3.2.4 XGBoost

XGBoost belongs to the boosting family, which is an engineering implementation of the GBDT algorithm. In the training process of the model, the residuals are focused, the second-order Taylor expansion is used in the objective function and the regularity is added. Then, we iterate through all the splitting points on all the features, calculate the gain of the objective function of all the samples split by these candidate splitting points, and find the feature with the largest gain and the candidate splitting point to split. In this way, the tree building process is completed layer by layer. XGBoost training is performed in an additive manner, that is, one tree is trained each time by focusing on the residuals, and the final prediction result is the sum of all trees.

XGBoost performs the selection of the optimal splitting points by first pre-sorting them and then calculating the gain of the objective function of all samples after the splitting of these splitting points for all splitting points of all features, a process with a large space complexity and time complexity.

The parameter of the XGBoost is shown in Table 3.4.

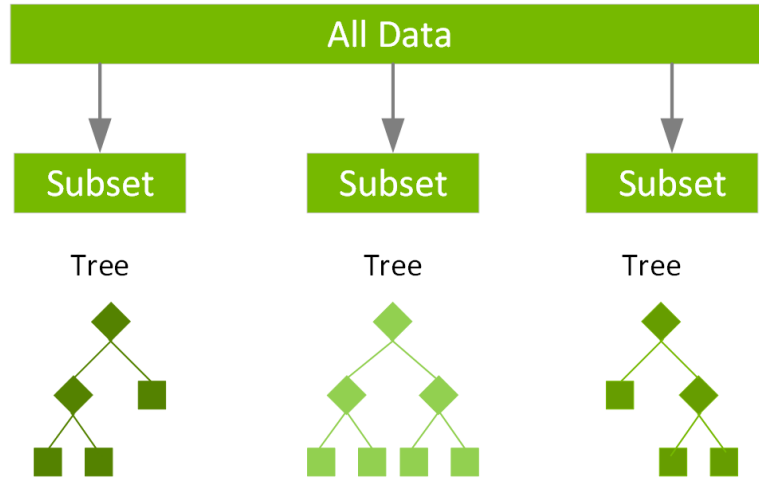


Figure 3.7: An Illustration of XGBoost

Table 3.4: Training parameters of XGBoost model.

Parameter	Definition	Value/Type
random_state	The seed of random number	0
scale_pos_weight	Determine the minimum leaf node sample weights sum.	10
learning_rate	Determine the step size at each iteration while moving toward a minimum of a loss function	0.1
max_depth	The maximum depth of the decision tree.	6
subsample	Control the proportion of random samples for each tree	0.8
min_child_weight	The sum of the minimum sample weights	10

### 3.2.5 AdaBoost

The basic principle of Adaboost algorithm is to combine multiple weak classifiers (weak classifiers are usually chosen as single-layer decision trees) in a reasonable way to make a strong classifier.

Adaboost adopts the idea of iteration, where only one weak classifier is trained in each iteration, and the trained weak classifier will be used in the next iteration. In other words, in the Nth iteration, there will be a total of N weak classifiers, of which N-1 are previously trained, and their various parameters are no longer changed, and the Nth classifier is trained this time. The relationship between the weak classifiers is that the Nth weak classifier is more likely to classify the data that the previous N-1 weak classifiers did not classify correctly, and the final classification output

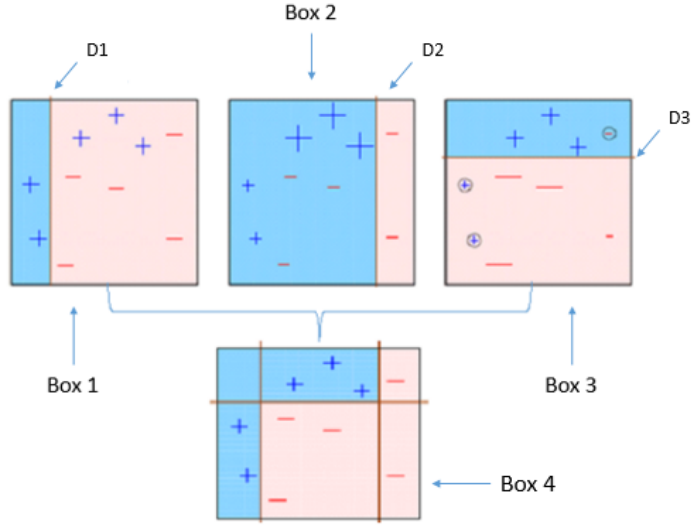


Figure 3.8: An Illustration of AdaBoost

depends on the combined effect of these N classifiers.

The parameter of the AdaBoost is shown in Table 3.5.

Table 3.5: Training parameters of AdaBoost model.

Parameter	Definition	Value/Type
random_state	The seed of random number	0
learning_rate	Determine the step size at each iteration while moving toward a minimum of a loss function	0.1
algorithm	The type of algorithm use in AdaBoost	SAMME.R

### 3.2.6 LightGBM

Most of the decision tree learning algorithms grow trees by level-wise strategy, remembering to split the leaves of the same level at a time and treating the leaves of the same level indiscriminately, while in fact many leaves have low splitting gain and no need for splitting, which brings unnecessary overhead. LightGBM grows the tree by a leaf-wise strategy. Each time, it finds the leaf with the greatest splitting gain from all the current leaves, and then splits it, and so on. Therefore, compared with Level-wise, Leaf-wise can reduce more errors and get better accuracy with the same number of splits. However, when the sample size is small, leaf-wise may cause

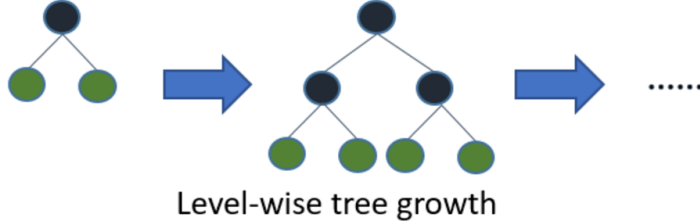


Figure 3.9: An Illustration of LightGBM

overfitting. Therefore, LightGBM can use the extra parameter  $max_{depth}$  to limit the depth of the tree and avoid overfitting.

The parameter of the LightGBM is shown in Table 3.6.

Table 3.6: Training parameters of LightGBM model.

Parameter	Definition	Value/Type
objective	Choose the objective function for training	multiclass
boosting_type	Choose the type of boosting	goss
num_leaves	Number of leaf nodes on a tree	10
max_depth	Maximum depth of the tree model	-1
learning_rate	a tuning parameter that determines the step size of each iteration	0.3
subsample	Control the proportion of random samples for each tree	800

### 3.2.7 Analysis and Conclusion

Generally, four machine learning models for posture recognition are put forwarded above. There are eight types of postures for classification, each type has a mount of 200 groups of data for training. For choosing classifier with the best performance, an analysis of training results is carried out in the following part.

#### 3.2.7.1 Confusion Matrix

The confusion matrix is a situation analysis table for summarizing the prediction results of a classification model in machine learning. The records in the data set are summarized in matrix form according to two criteria: the true category and the

category judgment predicted by the classification model. The rows of the matrix represent the true values and the columns of the matrix represent the predicted values. Figure 3.10 shows the confusion matrixes for six models implemented in ??.

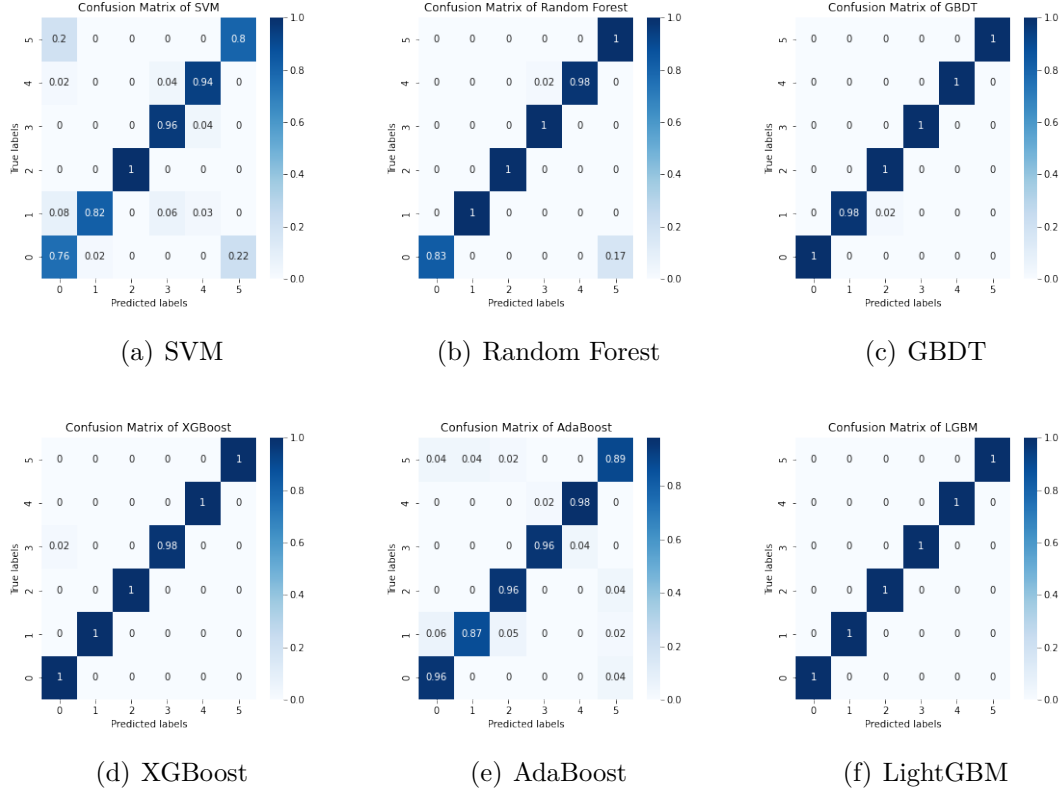


Figure 3.10: Confusion Matrixes of six models

### 3.2.7.2 Receiver Operating Characteristic Curve

The receiver operating characteristic curve (ROC curve) is also known as the sensitivity curve. The reason for this name is that the points on the curve reflect the same perceptivity, they are all responses to the same signal stimulus, but they are the result of several different criteria. The receiver operating characteristic (ROC) curve is a plot of the False Positive Rate (FPR) on the horizontal axis and the probability of hitting on the vertical axis, plotted against the different results obtained by the subject under a given stimulus condition using different judgment criteria.

The ROC curve is a curve based on a series of different dichotomies (cut-off values or decision thresholds), with the true positive rate (sensitivity) as the vertical

axis and the false positive rate (1-specificity) as the horizontal axis. The ROC curve evaluation method differs from the traditional evaluation method in that it does not require this restriction, but allows for intermediate states according to the actual situation, and the test results can be divided into several ordered categories, such as normal, approximately normal, suspicious, approximately abnormal and abnormal, before statistical analysis. Therefore, the ROC curve evaluation method is applicable to a wider range. Figure 3.11 shows the ROC curves for the six models.

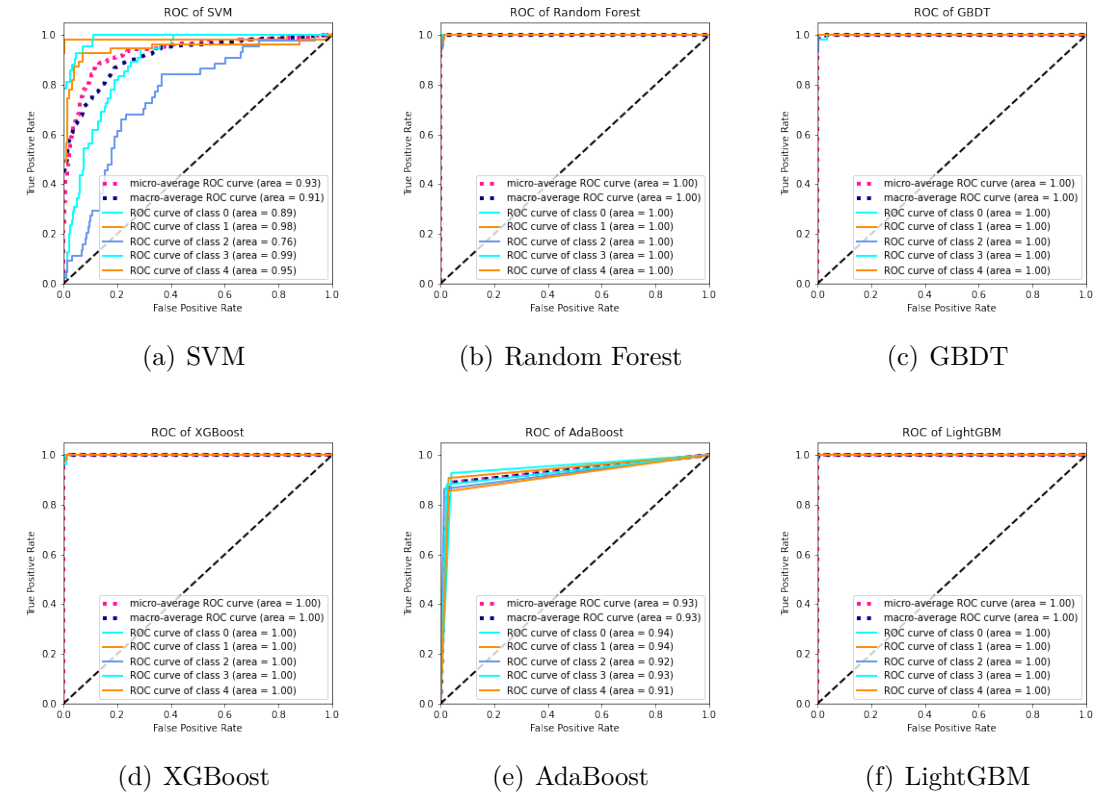


Figure 3.11: ROC Curve of six models

### 3.2.7.3 Learning Curve

The learning curve is the curve of the variation of the model's score on the training and validation sets for different training set sizes. The learning curve can help us to determine the current state of the model: overfitting or underfitting. Figure 3.11 shows the learning curves for the six models.

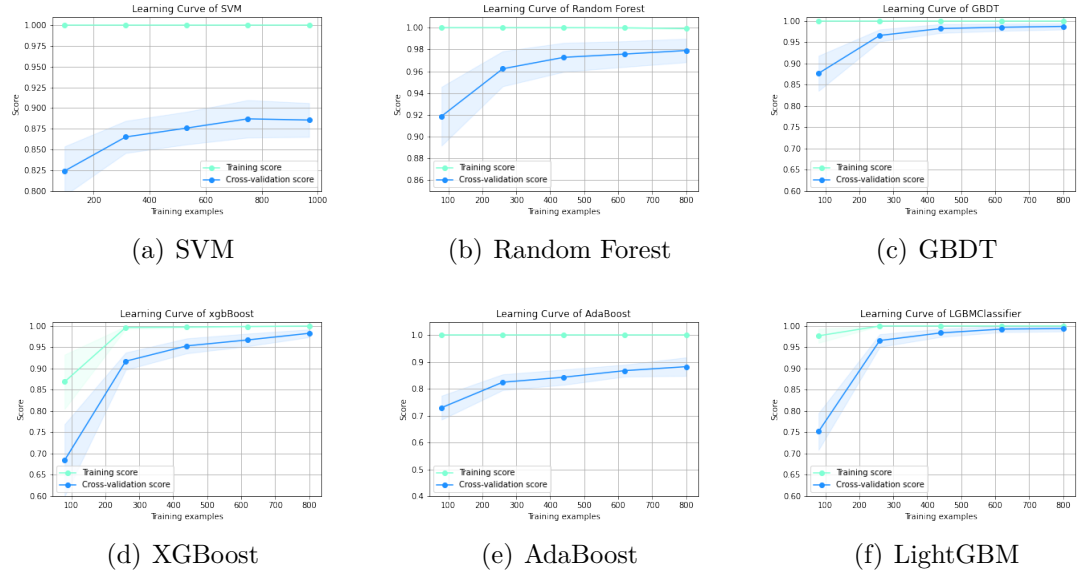


Figure 3.12: ROC Curve of six models

### 3.2.7.4 Comparison of Six Models

To choose the best model for body posture recognition, training results are collected below in and make a comparison. In the project, six different machine learning methods are used for exploring.

In § 3.2.7.1, we compared the confusion matrixes of six models. As we can find most of the models have accurate prediction for each type of motion except SVM has poor performance in type 0, 1 and 5 with relatively low accuracy. Besides, we can find that random forest have relatively weak performance in recognizing posture 0, and AdaBoost has relatively weak performance in recognizing posture 1.

In § 3.2.7.2, we make a comparison of the ROC curve of six models. As the figures indicates that only SVM and AdaBoost have a lower than 1 area both in micro-average and macro-average ROC curve, which represents the low accuracy of prediction.

In § 3.2.7.3, the learning curves of six models are compared. As the result shows that SVM model is under-fit. Because the training of SVM requires high uniformity of data, and two different kinds of sensors are combined in this project, the magnitude of the data they produce also differs greatly, so the training results are poor. Relatively the training process of XGBoost, GBDT, and LightGBM are well trained, as the training scores have reached 1.00 and cross validation scores are

also approaching 1.00. Especially, LightGBM has the best performance during the training process because of the sharp increase at the first 300 group of data.

Table 3.7 summarizes the performance metrics of each of these six models. Overall, LightGBM has the best performance, not only because of its 100% accuracy, but also because of its low computational complexity, which can complete the prediction of 300 sets of data in 0.01s, making it ideal for real-time posture prediction in this project.

Table 3.7: A Comparison among six models

Model	Accuracy	Macro-AUC	Micro-AUC	Training Time	Testing Time
SVM	88.15%	0.91	0.93	12.97 s	0.02 s
Random Forest	99.01%	1.00	1.00	11.46 s	0.03 s
GBDT	99.67%	1.00	1.00	277.62 s	0.02 s
XGBoost	99.67%	1.00	1.00	41.22 s	0.02 s
AdaBoost	93.42%	0.93	0.93	1.22 s	0.01 s
LightGBM	100.00%	1.00	1.00	6.05 s	0.01 s

### 3.2.8 Machine Learning on iPhone

In this project, we equip the LightGBM model in the iPhone for posture recognition. Apple, in combination with the built-in bionic chip, provides a machine learning interface in iOS development to transform models based on other AI frameworks (tensorflow, pytorch, scikit-learning, etc.) into a mlmodel format, which is suitable for the iPhone to be used in the app.

## 3.3 Database

In this report, we Adapt the Firebase database from google to implement the on-cloud data storage function for supporting the following cross-platform data storage and online medical diagnosis function.

Firebase Realtime Database is a cloud-hosted database. The database stores data as JSON and synchronizes with each connected client in real time. By using Firebase Realtime Database, different platforms share the same Realtime Database instance and enable automatic receipt of updated and up-to-date data.

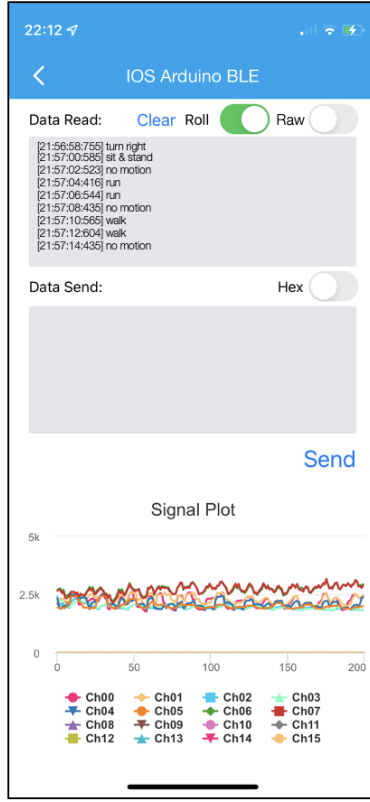


Figure 3.13: Realtime Posture Recognition on iPhone

Firebase Realtime Database stores data and synchronizes with NoSQL cloud databases. The data is synchronized across all clients in real time and remains available when the application is offline.

### 3.4 Web page

The web-based medical system was developed to facilitate doctors' access to patients' health status at all times and to enable easy cross-platform access mechanisms. The entire web Page includes three functions, authentication, data visualization and medical advice. For web development, we used the solution of Html5+Css3+JavaScript and deployed the web page to the private server based on tomcat container. And through the domain name resolution, so as to make quick access.

### 3.4.1 Authorization

In this report, due to the sensitivity of information about patients, data protection is needed to avoid the flow of private data and thus protect patient privacy.

Therefore, we added an authentication subpage to the project to ensure that only licensed physicians have access to the web data. Therefore, we added an authentication window when accessing the web page, and the logged-in person must register to log in to continue the access. Each physician account also has access to patient data under his name only, thus protecting patient privacy.

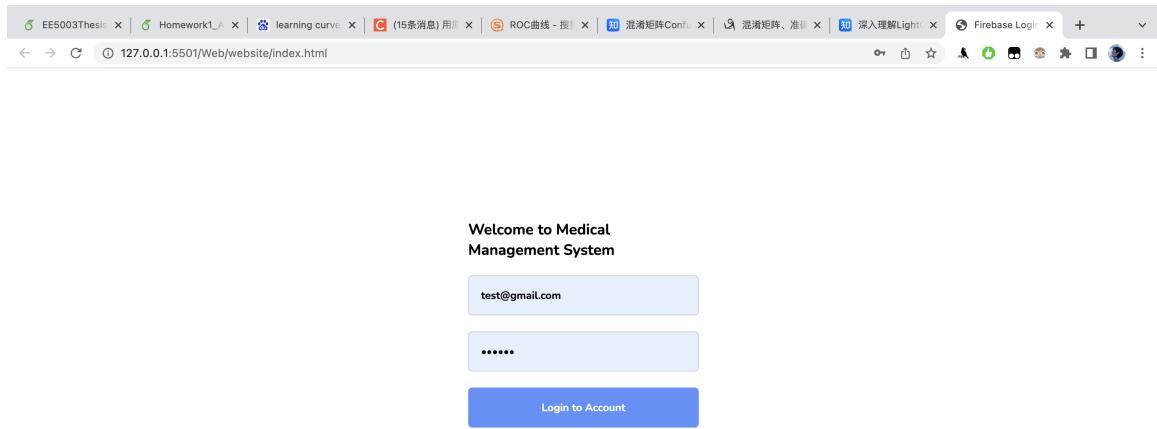


Figure 3.14: The Login Web Page

Firebase database provides abundant interfaces for authentication, here we only use email authentication login to ensure the identity management of the login. Figure 3.14 shows the login interface for user with the authenticated email.

### 3.4.2 Visualization

When a doctor logs on to our website, he can view the corresponding conditions by selecting different patients, patient's data can be retrieved from the Firebase database through JavaScript code. Combined with Css code, patient's data can be

## CHAPTER 3. BACK-END DESIGN

visualized and presented in the web page. By restricting the date, it is possible to do the analysis of the data for the specified date.

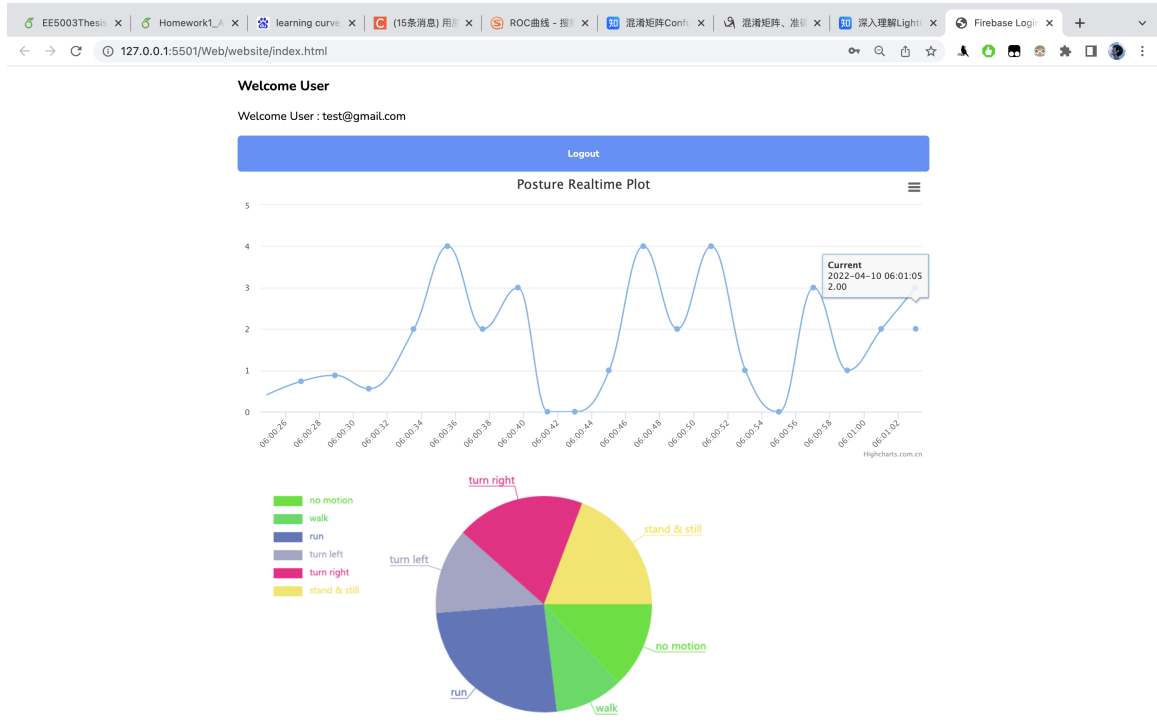


Figure 3.15: The Visualization Web Page

### 3.4.3 Medical Instruction

In order to facilitate doctors to give necessary medical advice to patients in a timely manner, we also provide a notification function on the webpage, through which doctors can send the advice they want to convey to patients and push it to their cell phones, and patients can also see the doctor's guidance on their cell phones

# Chapter 4

## Integration of System

The system framework design of the project is shown in Figure 4.1. First, we 3D printed an vest based on polyethylene material and combined two sensors, triboelectric and interdigital, to detect the patient's posture. In addition, we developed a signal acquisition communication module based on NRF52810 SoC to implement IoT functions.

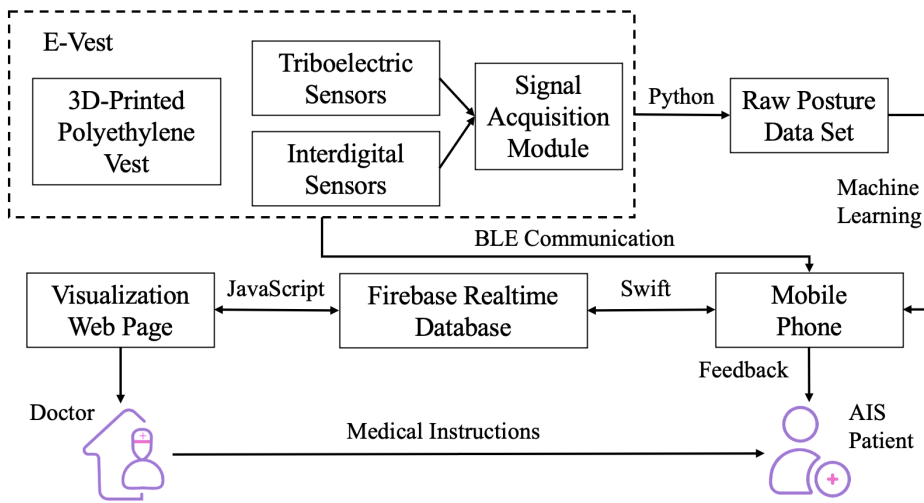


Figure 4.1: The Structure of the Medical Care System

In the back-end signal processing, we developed an app based on IOS platform for data reception, visualization, and machine learning to realize the intelligence of IoT. By combining database and web technologies, we developed a cross-platform online medical system to help doctors better analyze and diagnose patients' health conditions.

## CHAPTER 4. INTEGRATION OF SYSTEM

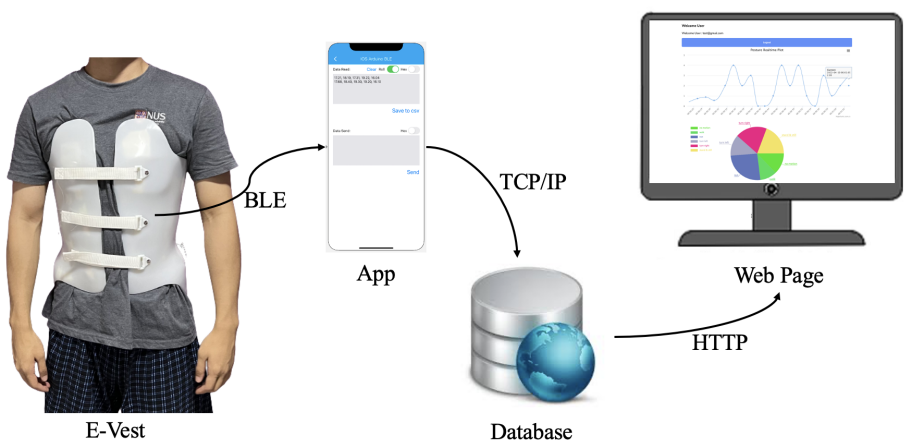


Figure 4.2: The Working Flow of the Medical Care System

# Chapter 5

# Conclusion and Future Work

## 5.1 Conclusion

In this project, a complementary medical treatment system was successfully constructed based on self-made wearable triboelectric and interdigital sensors.

First, a polyethylene-based, flexible, lightweight, low-cost, and comfortable lower-powered e-vest was manufactured and tested. Next, a signal acquisition systems was established, which helped the successful conversion from analog signals to digital signals and enabled wireless communication between e-vest and phone to be implemented. On this basis, the combination of AI algorithm and wearable sensor was explored, and the time-series data from the sensor was successfully processed. Additionally, a communication between phone and database is connected through TCP/IP, which realise the real-time data update. Lastly, a web page based on the database for visualization is implemented.

After all. this system we designed provides a closed-loop solution for monitoring, therapy, and diagnosis for adolescent scoliosis patients and doctors.

## 5.2 Further Research Directions

In this project, we developed a software based on iOS platform to receive and synchronize the data of e-vest. Although the market share of iPhone users is high, there are still a large number of Android phone users, and those who need to use our e-vest may not be using iOS platform. Therefore, we have considered developing a software based on Android platform in addition to supporting iOS devices, so as to achieve support for all mainstream cell phone systems and avoid inconvenience to

## CHAPTER 5. CONCLUSION AND FUTURE WORK

patients' operation. In addition, the current lab-made e-vest has a large number of exposed wires fixed by gluing. In order to ensure the stability of signal transmission and system power supply, we can use 3D printing technology to integrate the wiring into the e-vest in the subsequent production production to provide a more stable user experience.

In short, the work completed in this project explores the feasibility of integrating AI, cell phone, and wearable sensors in medical care application, which provides a solid foundation for subsequent research.

# Bibliography

- [1] S. Negrini, S. Donzelli, A. G. Aulisa, D. Czaprowski, S. Schreiber, J. C. de Mauroy, H. Diers, T. B. Grivas, P. Knott, T. Kotwicki, *et al.*, “2016 sosort guidelines: Orthopaedic and rehabilitation treatment of idiopathic scoliosis during growth”, *Scoliosis and spinal disorders*, vol. 13, no. 1, pp. 1–48, 2018.
- [2] S. L. Weinstein, L. A. Dolan, J. C. Cheng, A. Danielsson, and J. A. Morcuende, “Adolescent idiopathic scoliosis”, *The lancet*, vol. 371, no. 9623, pp. 1527–1537, 2008.
- [3] B. V. Reamy and J. Slakey, “Adolescent idiopathic scoliosis: Review and current concepts”, *American family physician*, vol. 64, no. 1, p. 111, 2001.
- [4] W. J. Shaughnessy, “Advances in scoliosis brace treatment for adolescent idiopathic scoliosis”, *Orthopedic Clinics of North America*, vol. 38, no. 4, pp. 469–475, 2007.
- [5] Y. Zhang, J. Liang, N. Xu, L. Zeng, C. Du, Y. Du, Y. Zeng, M. Yu, and Z. Liu, “3d-printed brace in the treatment of adolescent idiopathic scoliosis: A study protocol of a prospective randomised controlled trial”, *BMJ open*, vol. 10, no. 11, e038373, 2020.
- [6] S. Pasha, “3d spinal and rib cage predictors of brace effectiveness in adolescent idiopathic scoliosis”, *BMC musculoskeletal disorders*, vol. 20, no. 1, pp. 1–8, 2019.
- [7] A. Winter, S. Stäubert, D. Ammon, S. Aiche, O. Beyan, V. Bischoff, P. Daumke, S. Decker, G. Funkat, J. E. Gewehr, *et al.*, “Smart medical information technology for healthcare (smith)”, *Methods of information in medicine*, vol. 57, no. S 01, e92–e105, 2018.
- [8] M. Zhu, Z. Sun, T. Chen, and C. Lee, “Low cost exoskeleton manipulator using bidirectional triboelectric sensors enhanced multiple degree of freedom sensory system”, *Nature communications*, vol. 12, no. 1, pp. 1–16, 2021.

## BIBLIOGRAPHY

- [9] Q. Shi, C. Qiu, T. He, F. Wu, M. Zhu, J. A. Dziuban, R. Walczak, M. R. Yuce, and C. Lee, “Triboelectric single-electrode-output control interface using patterned grid electrode”, *Nano Energy*, vol. 60, pp. 545–556, 2019.
- [10] S. Viteckova, P. Kutilek, and M. Jirina, “Wearable lower limb robotics: A review”, *Biocybernetics and biomedical engineering*, vol. 33, no. 2, pp. 96–105, 2013.
- [11] R. R. Fletcher, M.-Z. Poh, and H. Eydgahi, “Wearable sensors: Opportunities and challenges for low-cost health care”, in *2010 Annual International Conference of the IEEE Engineering in Medicine and Biology*, IEEE, 2010, pp. 1763–1766.
- [12] N. D. Sidiropoulos, L. De Lathauwer, X. Fu, K. Huang, E. E. Papalexakis, and C. Faloutsos, “Tensor decomposition for signal processing and machine learning”, *IEEE Transactions on Signal Processing*, vol. 65, no. 13, pp. 3551–3582, 2017.
- [13] S.-p. Neuroprosthetics, H. Wang, T. Wu, and Q. Zeng, “A Review and Perspective for the Development of Triboelectric Nanogenerator ( TENG ) -Based”, *Micromachines*, 2020.
- [14] W. Ding, A. C. Wang, C. Wu, H. Guo, and Z. L. Wang, “Human–Machine Interfacing Enabled by Triboelectric Nanogenerators and Tribotronics”, Jan. 2019.
- [15] Z. L. Wang, “On maxwell’s displacement current for energy and sensors: The origin of nanogenerators”, *Materials Today*, vol. 20, no. 2, pp. 74–82, 2017.
- [16] O. Molnar, V. Gerasimov, and I. Kurytnik, “Triboelectricity and construction of power generators based on it”,, 2018.
- [17] M. Zhu, Z. Sun, Z. Zhang, Q. Shi, T. He, H. Liu, T. Chen, and C. Lee, “Haptic-feedback smart glove as a creative human-machine interface ( HMI ) for virtual / augmented reality applications”,, pp. 1–15, 2020.
- [18] F. Wen, Z. Sun, T. He, Q. Shi, M. Zhu, Z. Zhang, L. Li, T. Zhang, and C. Lee, “Machine Learning Glove Using Self-Powered Conductive Superhydrophobic Triboelectric Textile for Gesture Recognition in VR/AR Applications”, *Advanced Science*, vol. 7, no. 14, pp. 1–15, 2020, ISSN: 21983844.

## BIBLIOGRAPHY

- [19] K. Lakin, “Electrode resistance effects in interdigital transducers”, *IEEE Transactions on Microwave Theory and Techniques*, vol. 22, no. 4, pp. 418–424, 1974.
- [20] M. Khan, R. Rahaman, and S.-W. Kang, “Highly sensitive multi-channel idc sensor array for low concentration taste detection”, *Sensors*, vol. 15, no. 6, pp. 13 201–13 221, 2015.
- [21] S. M. Piryonesi and T. E. El-Diraby, “Data analytics in asset management: Cost-effective prediction of the pavement condition index”, *Journal of Infrastructure Systems*, vol. 26, no. 1, p. 04 019 036, 2020.
- [22] G. Biau, B. Cadre, and L. Rouvière, “Accelerated gradient boosting”, *Machine Learning*, vol. 108, no. 6, pp. 971–992, 2019.